The object of this study is the process of filtering astronomical frames that contain images of potential objects in the Solar System. To recognize the image of each such object in contrast with the background of the frame, it is necessary to carry out frequency filtering of the image. Any frequency filtering using various image filters is aimed at reducing the dynamic range of the background substrate. Also, frequency filtering leads to an increase in the signal-to-noise ratio of the entire image or its fragments, depending on the configuration. However, the identified problem area of each image during frequency filtering is the distortion of the structure of its edges. Therefore, to solve this problem, an edge effect compensation procedure has been proposed to eliminate structural distortions during frequency filtering.

Complementing the image with borders on all sides and the augmented extended image made it possible to introduce a formal connection between the pixel values of the extended image fragment and the pixel values of the extended original image. Testing was carried out using a high-pass Gaussian filter. The use of the devised edge effect compensation procedure made it possible to remove distortion of the structure of the image edges.

The devised edge effect compensation procedure was tested in practice within the CoLiTec project. It was implemented during the in-frame processing stage of the Lemur software.

The study showed that the use of the devised edge effect compensation procedure makes it possible to remove image artifacts compared to conventional filtering without taking into account the edge effect. Also, owing to edge effect compensation, structural image distortions were eliminated, and the signal-to-noise ratio was increased by 7–10 times

Keywords: high-pass filtering, Gaussian filter, edge effect, structure distortion, astronomical image

UDC 004.932.2

DOI: 10.15587/1729-4061.2024.308369

DEVISING AN EDGE EFFECT COMPENSATION PROCEDURE TO ELIMINATE STRUCTURAL DISTORTIONS DURING FREQUENCY FILTERING

Vladimir Vlasenko
PhD
Space Research and Communications Center
National Space Facilities Control and Test Center
Moskovska str., 8, Kyiv, Ukraine, 01010
Sergii Khlamov
Corresponding author
PhD, Test Automation Lead
SoftServe
Sadova str., 2D, Lviv, Ukraine, 79021
E-mail: sergii.khlamov@gmail.com
Vadym Savanevych
Doctor of Technical Sciences, Professor*
Oleksandr Vovk
PhD, Associate Professor
Department of Media Systems and Technologies**
Emil Hadzhyiev*
Yehor Bondar*
Yuriy Netrebin
Software Automation QA Engineer
INTIVE Limited
O'Connell Bridge House, D'Olier str., Dublin 2, Dublin, Ireland, D02RR99
*Department of Systems Engineering**
**Kharkiv National University of Radio Electronics
Nauky ave., 14, Kharkiv, Ukraine, 61166

Received date 03.05.2024
Accepted date 10.07.2024
Published date 30.08.2024

***How to Cite**: Vlasenko, V., Khlamov, S., Savanevych, V., Vovk, O., Hadzhyiev, E., Bondar, Y., Netrebin, Y. (2024). Devising an edge effect compensation procedure to eliminate structural distortions during frequency filtering. Eastern-European Journal of Enterprise Technologies, 4 (2 (130)), 30–39. https://doi.org/10.15587/1729-4061.2024.308369*

1. Introduction

The active development of the field of observational astronomy [1] continues due to the constant improvement of various methods of astrometry [2] and photometry [3]. Owing to continuous breakthroughs in telescope construction and digital technologies, astronomical data are gradually becoming big data [4]. They have a high resolution of the original frames in series and require a huge amount of memory, both physical for storage and operational for processing. The generation of such large astronomical data is carried out using large asteroid surveys consisting of several telescopes equipped with very large charge-coupled device (CCD) cameras [5]. During any type of processing (intra-frame or inter-frame) of such big data, huge astrometric and photometric catalogs with guide stars, as well as archival big data, are still involved [6]. That is making it possible to accumulate, obtain knowledge [7], and analyze accumulated publicly available data [8], as well as measurements for each object. Typically, astronomical data are classified according to specific features/patterns [9], belonging to different classes/types of Solar System Objects (SSOs) (for example, asteroids or comets), as well as artificial Earth satellites. Such measurements were obtained over a long observation period and their analysis may even include calculation of the period and shape of rotations of such SSOs [10].

To recognize the image of each such SSO in contrast with the background of the frame, it is recommended to carry out

frequency filtering of the image. This is part of the preparatory intra-frame processing of the source frame, allowing for brightness leveling of the background. Pre-obtained calibration frames from telescopes are also used to remove hot/cold pixels and partial artifacts from the optical system.

Any frequency filtering using various image filters is aimed at reducing the dynamic range of the background substrate. Also, frequency filtering leads to an increase in the signal-to-noise ratio of the entire image or its fragments, depending on the configuration.

The relevance of constantly improving methods for frequency filtering of digital frames is related to the desire to increase the accuracy of subsequent assessment of the brightness and positional coordinates of objects under study [11]. Also of interest is the increase in the conditional probability of correct detection (CPCD) of real objects [12] under the mode of their tracking.

2. Literature review and problem statement

One of the key problems in the field of processing astronomical frames is the poor quality of images of objects in the frame. This leads to heterogeneity in the typical shape of object images [13]. The typical shape directly depends on the conditions and quality of shooting with a CCD camera. There are many external factors that affect the quality of shooting, such as vignetting, hot/cold pixels, structural distortion, and optical system artifacts [14]. The typical shape is an important factor that influences the subsequent process of detecting objects and estimating their position and brightness. Methods for preliminary image preparation were considered that can remove artifacts and shift the positional coordinates of the frame center between frames in a series, as well as level the brightness of the background.

The main disadvantage of computer vision methods [15] is that they are not able to accurately outline images of objects with a non-standard standard shape. Any changes in background brightness or stray flares significantly affect CPCD.

Classical methods for object image recognition [16] require analysis of all pixels of potential SSOs to determine their typical shape. In the case of heterogeneity of the standard form, objects are mixed up. And in the case when the standard form is non-standard, such methods cannot select the required recognition pattern, which leads to the loss of the object or false detection of the object.

In [17], the authors use automatic selection of a reference point to select calibration frames as preprocessing. This algorithm involves first analyzing the image to find reference points and then identifying it with astronomical catalogs. If there are artifacts in the images, these control points may be false, which makes it impossible to execute the algorithm.

The classical Kalman filter is also known, which is designed for recursive estimation of the state vector of an a priori known dynamic system [18]. To calculate the current state of the system, it is necessary to know the current measurement, as well as the previous state of the filter itself. The disadvantage is that in the presence of stray light, the brightness of the potential measurement pixel may be blocked by the brightness of the background substrate.

Paper [19] proposes a framework for detecting and correcting wide-angle optical aberrations based on deep learning. This model uses two modules that take a set of three phase-separated images and estimate the phase of the wavefront in terms of its constituent coefficients. The disadvantage of this framework is the lengthy process of deep learning. It is also impossible to predict in advance what kind of aberrations or artifacts there may be in an optical system.

A matched filtering algorithm is also known [20, 21], but it uses only an analytical image model. The disadvantage of this algorithm is that the analytical model can only be applied to those typical forms of objects that can be described by standard mathematical expressions. In the case where the standard form is non-standard, the analytical model no longer works.

The identified problem area of each image during frequency filtering is the distortion of the structure of its edges due to the characteristics of the observing conditions or the optical system.

Based on the above, all existing image preprocessing methods are not adapted to work with images with structural distortions caused by aberrations of optical systems. Another disadvantage is the inability to have one algorithm for leveling the brightness of the substrate background in the event of stray light or artifacts.

Therefore, it is necessary to devise a procedure for compensating for the edge effect. It will make it possible to eliminate structural distortions during image processing by high-pass filtering. This will also lead to an increase in the signal-to-noise ratio throughout the frame, as well as for each segment/fragment of the frame in the case of splitting.

3. The aim and objectives of the study

The purpose of our study is to eliminate structural distortions during image processing by high-pass filtering. From a practical point of view, this will make it possible to increase the degree of uniformity of the background component and, accordingly, the signal-to-noise ratio.

To achieve the goal, the following tasks were set:

– to add borders to the image of the original frame;

– to introduce a formal connection between the pixel values of the image of the original and extended frames;

– to develop an algorithm for the edge effect compensation procedure;

– to verify the edge effect compensation procedure.

4. The study materials and methods

The object of our study is the process of frequency filtering of astronomical frames that contain SSO images. The work proposes to test the working hypothesis that when adding borders to the original image and subsequent high-frequency filtering, the edge effect will be compensated. It was hypothesized that to compensate for the edge effect, structural distortions and artifacts could be eliminated, which would lead to an increase in the signal-to-noise ratio. The work also adopted a simplification, which is associated with the uniformity of the standard form of images of all objects in the frame and the absence of their synchronous blur.

The Gaussian filter [22] was chosen as the high-pass filtering method used in the paper. This filter was selected based on comparison with other similar filters, where experimental studies revealed that the impulse response of this filter does not have concentric rings. Therefore, the resulting images after filtering with a Gaussian filter also lack ringing artifacts [23].

The statistical method was chosen as a theoretical research method. This method was chosen for preliminary testing of the hypothesis put forward before full-scale experiments to confirm the correctly selected filter. The choice of the statistical method was based on a comparison of the variances and standard deviations of the brightness estimates of peak images of potential objects obtained by different filters to select the best filter [23].

The work used an efficiency criterion, which was calculated as the degree of uniformity of the background component. On a whole original frame with an uneven background, the average background brightness values of the segments will vary from segment to segment across the frame [24]. The greater the unevenness of the background of the digital frame, the wider the scope of these changes will be. Therefore, the range of average background brightness values of digital frame segments was used as a value characterizing the degree of uniformity of the background component.

As an experimental study, full-scale experiments were carried out, in which the initial test series were acquired from various telescopes installed at observatories in Ukraine and around the world. Namely, the ISON-NM observatory, the SANTEL-400AN telescope (New Mexico, USA); National Astronomical Research Institute of Thailand (NARIT, Thailand) [25], Vihorlat Observatory, VNT telescope (Humenne, Slovakia) [26]; Odesa-Mayaky observatory, OMT-800 telescope (Mayaki, Ukraine) [27], Takahashi BRC-250M (Uzhgorod, Ukraine) [28].

The observation conditions for the experiments were specially chosen so that the resulting series of frames contained a variety of typical forms of object images and structural distortions with artifacts. The original astronomical frames considered for the study had a variety of resolutions, namely: 512×512, 768×512, 3056×3056, and 4008×2672 pixels.

The devised procedure for compensating for the edge effect was implemented in the C++ programming language. This code was used at the stage of preliminary processing of the Lemur software package (Ukraine) [29] for the automated detection of new and tracking of known objects within the CoLiTec project [30]. The devised procedure, implemented in the Lemur software (Ukraine), was used during the successful processing of astronomical frames, which contained a total of more than 800,000 SSOs. Their measurements were also successfully identified with known astronomical catalogs. With this fact, the procedure for compensating for the edge effect confirmed its practical necessity within the framework of the main hypothesis put forward.

5. Results of investigating the edge effect compensation procedure

5. 1. Adding borders to the image of the original frame

The accuracy of brightness estimation and object detection deteriorates significantly with a certain feature of the formation of astronomical frames – vignetting. This is a structural distortion and artifact, which is characterized by a gradual decrease in image brightness from the center to the edges of the field of view of the optical system, which reduces the signal-to-noise ratio (SNR) of object images (Fig. 1).

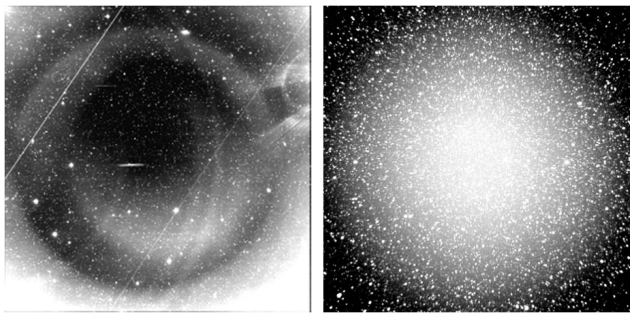

a *b*

Fig. 1. Examples of an astronomical frame: *a* — with structural distortion; *b* — with an artifact (stray light exposure)

Forward and inverse two-dimensional discrete Fourier transform (DFT) is defined for periodic images [31]. In this regard, fragments of image A_{crkl} are proposed to be represented as periodic images with a period N_{crx} along the abscissa axis and N_{cry} along the ordinate axis. Formally, to be able to use Fourier analysis in practice, an infinite image is introduced that repeats a fragment of the image vertically and horizontally (Fig. 2).

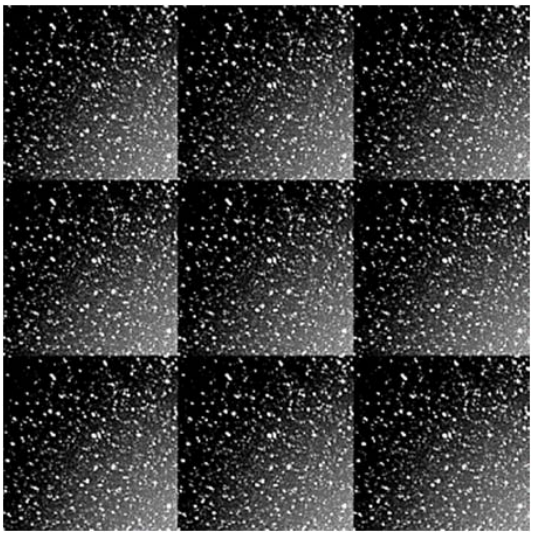

Fig. 2. An example of a formally infinite image of an astronomical frame with structural distortion and artifact (stray flare)

This formally infinite image, corresponding to an image fragment, is synthesized in such a way that the right edge of the image fragment is adjacent to the left edge of the same fragment, and the top edge is adjacent to the bottom. Due to discontinuities in brightness values, at the points of contact of previously introduced image fragments, additional harmonics appear in the spectrum of an infinite image, lying on the coordinate axes of the frequency plane of the image fragment spectrum (Fig. 3). These harmonics correspond to sharp changes in brightness at the border of an image fragment. As a result, when frequency filtering an image, its structure at the edges is distorted.

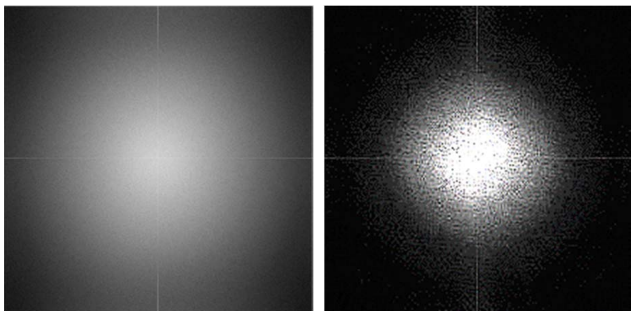

a *b*

Fig. 3. Examples of spectra of a fragment of an infinite image of an astronomical frame: *a* — with structural distortion; *b* — with an artifact (stray light exposure)

The original frame A_{in} of size $N_{CCDx}\times N_{CCDy}$ is divided into $M_x\times M_y$ fragments A_{crkl} of size $N_{crx}\times N_{cry}$ (Fig. 4, *a*).

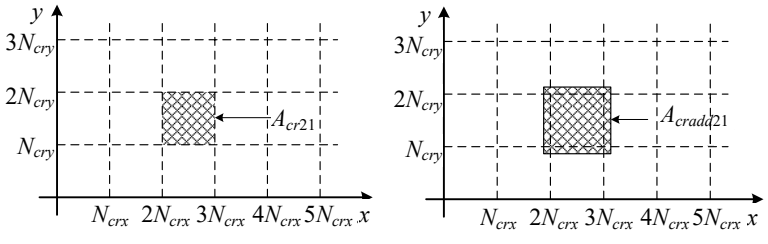

a *b*

Fig. 4. Covering the original frame: *a* — fragments; *b* — fragments with borders

To compensate for the edge effect, image fragments are supplemented with a border on the left, right, top, and bottom (Fig. 4, *b*). In this case, the border pixel values depend on which border of the image fragment the border is adjacent to.

If the border of an image fragment lies inside the original image, then the border is the corresponding pixels of the adjacent image fragment, which are a natural continuation of the fragment under study.

The width of the border N_{ADDx} and N_{ADDy}, which complements the image fragments and the original image on the left – right and top – bottom, are determined from the following expression:

$$N_{ADDx}=\frac{M_{hx}-1}{2}, \quad (1)$$

$$N_{ADDy}=\frac{M_{hy}-1}{2}, \quad (2)$$

where M_{hx}, M_{hy} are the dimensions of the region along the abscissa and ordinate axis, within which the impulse response of the high-frequency filter is not equal to zero.

In the case where the boundary of the image fragment is the boundary of the original image, an expanded original image A_{inadd} of size $(N_{CCDx}+2N_{ADDx})\times(N_{CCDy}+2N_{ADDy})$ is obtained from the original image A_{in} by adding a border on the side of each of the boundaries of the original image A_{in}. The values of the image border pixel and the image pixel are equal when they are symmetrically placed relative to the nearest border of the image in question. This rule is formalized by the expressions given below.

The pixel values of the border of the original image A_{in} on the left are equal to the pixel values of the original image A_{in} located symmetrically to the left border of the image, according to the following expression:

$$A_{inadd}(m, n)=A_{in}(N_{ADDx}-m-1, n), \quad (3)$$

where $m=\overline{0,N_{ADDx}-1}$, $n=\overline{N_{ADDy},N_{CCDy}+N_{ADDy}-1}$.

The pixel values of the border of the original image A_{in} on the right are equal to the pixel values of the original image A_{in} located symmetrically to the right border of the image, according to the following expression:

$$A_{inadd}(m, n)=A_{in}(2N_{CCDx}+N_{ADDx}-m-1, n), \quad (4)$$

where:

$$m=\overline{N_{CCDx}+N_{ADDx},N_{CCDx}+2N_{ADDx}-1},$$

$$n=\overline{N_{ADDy},N_{CCDy}+N_{ADDy}-1}.$$

The values of the border pixels of the original image A_{in}, located at the bottom of the image, as well as in the lower left and right corners of the image, can be expressed in terms of the pixel values of the extended original image A_{inadd} according to the following expression:

$$A_{inadd}(m, n)=A_{in}(m, 2N_{ADDx}-n-1), \quad (5)$$

where $m=\overline{0,N_{CCDx}+2N_{ADDx}-1}$, $n=\overline{0,N_{ADDy}-1}$.

The values of the border pixels of the original image A_{in}, located on the top of the image, as well as in the upper left and right corners of the image, can be expressed in terms of the pixel values of the extended original image A_{inadd} according to the following expression:

$$A_{inadd}(m, n)=A_{inadd}(m, 2(N_{CCDy}+N_{ADDx})-n-1), \quad (6)$$

where:

$$m=\overline{0,N_{CCDx}+2N_{ADDx}-1},$$

$$n=\overline{N_{CCDy}+N_{ADDy},N_{CCDy}+2N_{ADDy}-1}.$$

An example of the original image A_{in} and the extended original image A_{inadd} are shown in Fig. 5.

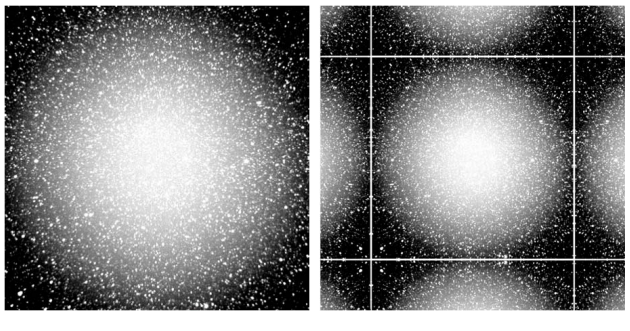

a *b*

Fig. 5. Example of an astronomical image: *a* — original; *b* — original image expanded with borders

After introducing the extended source image, it is also necessary to introduce a formal connection between the pixel values of the image of the original and extended frames.

5. 2. Formal connection between the pixel values of the image of the original and extended frames

To introduce a formal connection between the pixel values of the image of the original and extended frames, it is necessary to obtain all the pixels belonging to the original image, as well as the pixels of the extended original image. It is also necessary to take into account the peculiarities of dividing the original image into fragments, taking into account borders.

The pixel values of the extended source image A_{inadd} with numbers:

$$m=\overline{N_{ADDx},N_{CCDx}+N_{ADDx}-1},$$

and

$$n=\overline{N_{ADDy},N_{CCDy}+N_{ADDy}-1},$$

are related to the pixel values of the source image A_{in} via the following expression:

$$A_{inadd}(m,n)=A_{in}(m-N_{ADDx},n-N_{ADDy}). \quad (7)$$

After introducing the extended source image A_{inadd}, a formal connection is introduced between the pixel values of the k*l*-th extended image fragment $A_{craddkl}$ and the pixel values of the extended source image A_{inadd} according to the following expression:

$$A_{craddkl}(m,n)=A_{inadd}(m+N_{crx}k,n+N_{cry}l), \quad (8)$$

where $m=\overline{0,N_{crx}-1}$, $n=\overline{0,N_{cry}-1}$, $k=\overline{0,M_x-1}$ and $l=\overline{0,M_y-1}$.

As a result of high-frequency filtering of the *kl*-th extended image fragments $A_{craddkl}$, the *kl*-th filtered extended image fragments $A_{outaddkl}$ are obtained. The filtered image A_{out} is formed from the resulting fragments. The pixel values of the filtered image A_{out} are related to the pixel values of the *kl*-th filtered extended image fragments $A_{outaddkl}$ according to the expression:

$$A_{out}(m,n)=A_{outaddkl}(m+N_{ADDx}-kN_{crx},n+N_{ADDy}-lN_{cry}), \quad (9)$$

where $A_{outaddkl}(m,n)$ – pixel values of the *kl*-th filtered extended image fragment, with $m=\overline{0,N_{CCDx}-1}$, $n=\overline{0,N_{CCDy}-1}$ and $k=E\left[\frac{m}{N_{crx}}\right]$, $l=E\left[\frac{n}{N_{cry}}\right]$.

The resulting formal connection will make it possible to obtain the pixel values of a filtered and brightness-leveled image without borders after performing high-pass filtering.

5. 3. Development of an algorithm for the edge effect compensation procedure

The proposed algorithm for the edge effect compensation procedure includes the following sequence of operations:

1. Obtaining the dimensions $N_{CCDx}\times N_{CCDy}$ of the original frame in pixels.

2. Formation of a discrete spectrum of the original astronomical frame S_{in} using direct DFT of the original astronomical frame A_{in}:

$$S_{in}(u,v)=\sum_{m=0}^{N_{CCDx}-1}\sum_{n=0}^{N_{CCDy}-1}A_{in}(m,n)exp\left(\begin{matrix}-i\frac{2\pi}{N_{CCDx}}mu-\\-i\frac{2\pi}{N_{CCDy}}nv\end{matrix}\right), \quad (10)$$

where $S_{in}(u, v)$ is the uv-th harmonic of the discrete spectrum of the source frame;

$A_{in}(m, n)$ – brightness of the mnth pixel of the source frame.

3. Dividing the original frame into N_s segments/fragments of the same size $N_{sx}\times N_{sy}$ pixels.

4. Determining the width of the border, which complements the image fragments and the original image from left to right (1) and top to bottom (2).

5. Adding a border to each frame segment and determining the pixel values on each side (3) to (6).

6. Introduction of a formal connection (7) of the pixel values of the extended source image A_{inadd} with the pixel values of the source image A_{in}.

7. Introduction of a formal connection (8) of the pixel values of the *kl*-th extended image fragment $A_{craddkl}$ with the pixel values of the extended original image A_{inadd}.

8. Selection of the transfer function H_{Ghp} of the high-frequency Gaussian filter [32]:

$$H_{Ghp}(u,v)=1-exp\left(-\frac{r^2(u,v)}{2\sigma_\omega^2}\right), \quad (11)$$

where σ_ω is the shape parameter of the transfer function of the high-frequency Gaussian filter;

$r(u,v)=2\pi\sqrt{\left(u-E[N/2]\right)^2/N^2+\left(v-E[M/2]\right)^2/M^2}$ – distance from the point (u, v) of the frequency domain to the origin of the spectrum;

u, v – numbers of frequency components of the spectrum $u=\overline{0,N-1}$, $v=\overline{0,M-1}$;

$M\times N$ – the size of the filter transfer function, equal to the size of the image spectrum over which high-frequency filtering is performed.

9. Performing a high-pass filtering procedure for each *kl*-th extended fragment.

10. Obtaining (9) pixel values of the filtered image A_{out} with the pixel values of the *kl*-th filtered extended image fragments $A_{outaddkl}$.

5. 4. Verification of the edge effect compensation procedure

To verify the devised edge effect compensation procedure, testing was carried out on a series of frames obtained from various telescopes. A Gaussian filter was chosen as a high-pass filter.

To uniformly determine the quality indicators of high-frequency filtering, a digital frame was considered, divided into N_s segments/fragments of the same size $N_{sx}\times N_{sy}$ pixels. In each segment, the average value and standard deviation (RMS) $\sigma_{\Theta s}$ of the background brightness were calculated on the set of background pixels Θ_s of the *s*-th studied segment of the digital frame:

$$\bar{A}_{\Theta s}=\sum_{m,n\in\Theta s}A_s(m,n)/N_{\Theta s}, \quad (12)$$

$$\sigma_{\Theta s}=\sqrt{\sum_{m,n\in\Theta s}A_s(m,n)^2/(N_{\Theta s}-1)-\left(\sum_{m,n\in\Theta s}A_s(m,n)/(N_{\Theta s}-1)\right)^2}, \quad (13)$$

where $A_s(m, n)$ is the brightness of the pixel with numbers m, n of the sth frame segment;

m, n – pixel numbers of the s-th frame segment along the abscissa and ordinate $m = \overline{0, N_{sx} - 1}$, $n = \overline{0, N_{sy} - 1}$;

$N_{sx} \times N_{sy}$ – size of the -th frame segment along the abscissa and ordinate;

$N_{\Theta s}$ – number of pixels in the background of the -th segment of the digital frame.

On a whole original frame with an uneven background (with structural distortions and artifacts), the average background brightness values $\overline{A}_{\Theta s}$ of the segments will vary from segment to segment across the frame. The greater the unevenness of the background of the digital frame, the wider the scope of these changes will be. Therefore, the value characterizing the degree of uniformity of the background component is the range R_{aver} of the average values $\overline{A}_{\Theta s}$ of the background brightness of the digital frame segments:

$$R_{aver} = \overline{A}_{\Theta \max} - \overline{A}_{\Theta \min}, \quad (14)$$

where $\overline{A}_{\Theta \min}$, $\overline{A}_{\Theta \max}$ are the minimum and maximum values of the average background brightness values of frame segments.

The result of high-frequency filtering of the original image (Fig. 5) when expanding image fragments is shown below in Fig. 6. The original image was divided into nine fragments. High-frequency filtering of the obtained image fragments without taking into account the edge effect leads to the appearance of artifacts in the filtered image. These artifacts are located along the lines of dividing the image into fragments (Fig. 6, *a*). When using the edge effect compensation procedure, there are no artifacts in the filtered image (Fig. 6, *b*).

Below, Table 1 gives the obtained indicators of the quality of alignment of astronomical digital frames using the example of a series of four frames. These values were calculated for digital frames measuring 1528×1528 pixels and divided into segments of 30×30 and 50×50 pixels.

Below, Fig. 7–10 show histograms of the range of average background pixel brightness values and the average standard deviation of background pixel brightness in segments of 30×30 and 50×50 pixels.

The results of our study, shown in Fig. 6–10, *b*, and given in Table 1, indicate successful verification of the devised procedure and confirmation of the working hypothesis put forward.

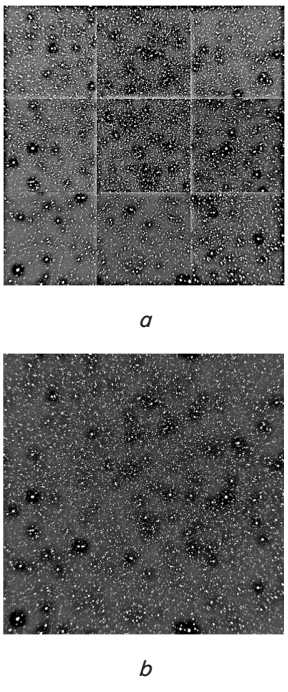

a

b

Fig. 6. The result of high-frequency filtering of the original image: *a* – without taking into account the edge effect; *b* – taking into account the edge effect

Table 1

Luminance alignment quality indicators for four frames

Frame number		The range of the average background brightness values of the segments, R_{aver}, ADU		Average of background pixel brightness segments by RMS segments, $\overline{\sigma}_{\Theta}$, ADU	
		Segment size			
		30×30	50×50	30×30	50×50
1	Original	1503.76	1483.03	40.42	44.84
	After filtration	85.65	55.13	37.58	37.57
2	Original	1518.94	1493.48	40.26	44.65
	After filtration	103.85	55.32	37.45	37.45
3	Original	1537.46	1490.36	40.39	44.81
	After filtration	91.51	51.68	37.56	37.57
4	Original	1708.48	1563.45	40.35	44.69
	After filtration	277.49	134.95	37.58	37.58

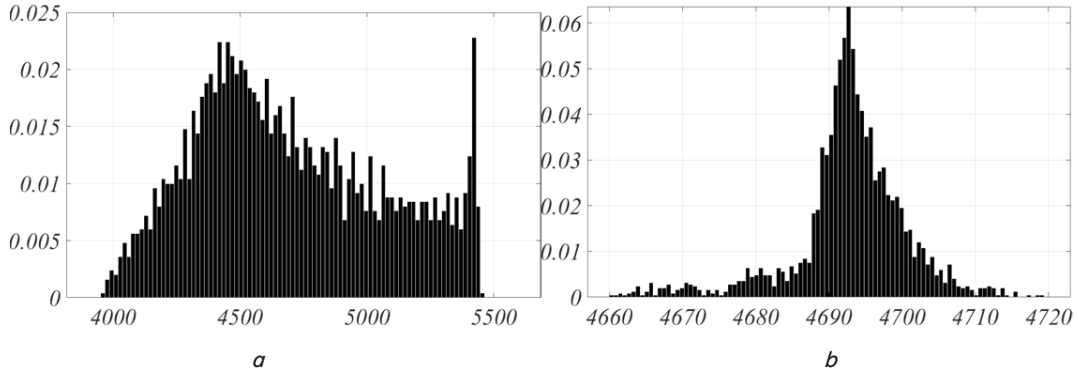

a *b*

Fig. 7. Histogram of the range of average brightness values of background pixels in segments of 30×30 pixels: *a* – original image; *b* – aligned image

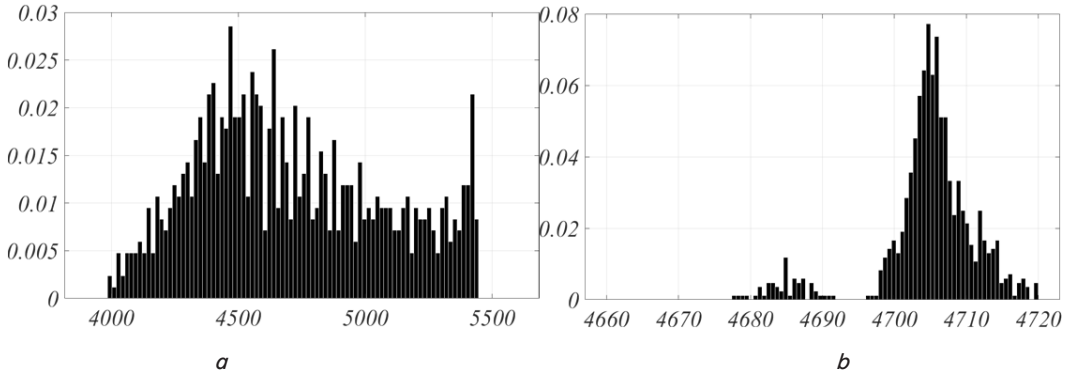

Fig. 8. Histogram of the range of average brightness values of background pixels in segments of 50×50 pixels: *a* – original image; *b* – aligned image

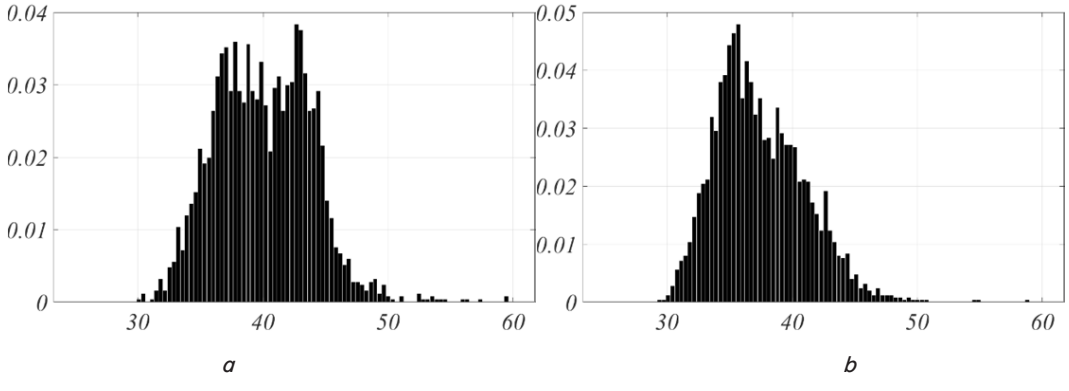

Fig. 9. Histogram of the average standard deviation of the brightness of background pixels in segments of 30×30 pixels: *a* – original image; *b* – aligned image

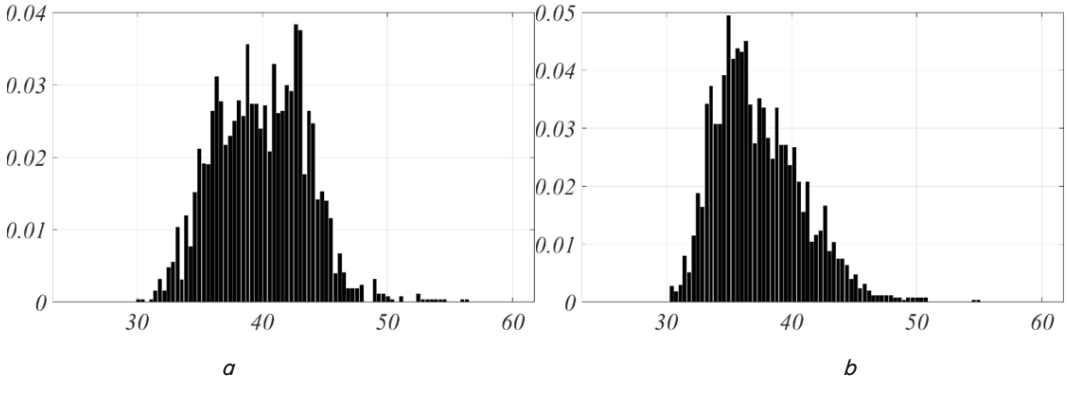

Fig. 10. Histogram of the average standard deviation of the brightness of background pixels in segments of 50×50 pixels: *a* – original image; *b* – aligned image

6. Discussion of results of investigating the edge effect compensation procedure

Within the framework of the CoLiTec project [33] and Lemur software (Ukraine), a study was carried out on the edge effect compensation procedure to eliminate structural distortions (Fig. 1) during frequency filtering.

Using the properties of forward and inverse two-dimensional DFT, a formal infinite image was introduced, repeating a fragment of the image vertically and horizontally (Fig. 2). Adding borders on each side of the fragment (3) to (6) made it possible to supplement the pixels of the fragments with pixels of repeating fragments for uniform distribution of the background substrate during further frequency filtering (Fig. 4, 5, *b*).

The introduction of a formal connection between the pixel values of extended image fragments and the pixel values of the extended original image made it possible to link image pixels. Also, owing to the introduced formal connection, it became possible to obtain the pixel values of the filtered and brightness-leveled image (9) without borders after performing high-frequency filtering.

A key aspect of the developed algorithm for the edge effect compensation procedure is the application of the

Gaussian filter transfer function (11) to the border-expanded formal infinite image for high-pass filtering.

Analysis of the introduced quality indicators for alignment of astronomical digital frames indicates that as a result of high-frequency filtering, the signal-to-noise ratio of frame segments is reduced by 7–10 times (Table 1). This indicates that the use of the devised edge effect compensation procedure made it possible to remove the distortion of the structure of the image edges.

The range of average background pixel brightness values decreases by 15 times for segments of 30×30 pixels and by 23 times for segments of 50×50 pixels (Fig. 7, 8). In this case, the segment-average standard deviation of the brightness of the background pixels in the segments under study does not change significantly. Specifically, 1.1 times for brightness values calculated in segments of 30×30 pixels and 1.2 times for segments of 50×50 pixels (Fig. 9, 10).

Statistical and full-scale modeling [34] have proven that this also significantly affects the accuracy of a number of tasks of brightness leveling, accumulation and data acquisition [35].

A limitation of our study is the integrity of the astronomical frame file and the restriction of read/write access to the file. Also important is the issue of file security, namely encryption of input data. In this case, an additional decryption algorithm will be required.

The disadvantage of the study is that the proposed edge effect compensation procedure cannot be used in the case of gradual or online acquisition of astronomical frames from telescopes. In this case, access to the file is blocked, and only after the file is completely formed and saved is the blocking removed. And this will already make it possible to successfully apply the devised procedure and begin frequency filtering.

It is advisable to focus further research on the use of the devised edge effect compensation procedure in combination with other high-frequency filters (for example, an ideal filter or a Butterworth filter). Also interesting from a practical point of view will be the application of the devised procedure not only to the initial astronomical target frames but also to calibration service frames.

7. Conclusions

1. Forward and inverse 2D DFT has been defined for periodic images. This feature made it possible to introduce a formal infinite image that repeats a fragment of the image vertically and horizontally. It was proposed to add borders on each side of the fragment, which made it possible to supplement the pixels of the fragments with pixels of repeating fragments for uniform distribution of the background substrate during further frequency filtering. To prepare for high-pass filtering, the pixel values of the borders on each side of the original image fragment were determined. This allowed the original image to be expanded by 0.5 to 1.5 times to perform frequency filtering to flatten the background substrate.

2. A formal connection was introduced between the pixel values of image fragments expanded by 0.5–1.5 times with the pixel values of the expanded original image. After performing high-pass filtering, this made it possible to obtain the pixel values of a filtered and brightness-leveled image without borders.

3. An algorithm for the edge effect compensation procedure has been developed. The key point is to take into account the peculiarities of the formation of fragments depending on the size of the frame with the subsequent formation of the spectrum of the high-frequency component of the image based on the selected transfer function. This made it possible to perform high-pass filtering of each fragment, and to assemble an output filtered image without borders with a signal-to-noise ratio increased by 7–10 times.

4. The devised edge effect compensation procedure was verified using a high-frequency Gaussian filter based on many series of frames of different sizes. Owing to the introduction of extended borders to fragments of the original frame, as well as the clarification of the formal connection between the pixel values of the filtered frame and its extended fragments, the use of the devised procedure increased the signal-to-noise ratio by 7–10 times. Verification of the devised procedure also showed a significant decrease in the range of average pixel brightness values by tens of times. Visual verification demonstrated compensation for the edge effect, structural distortions, flare, and artifacts after applying the devised procedure and high-frequency filtering.

Conflicts of interest

The authors declare that they have no conflicts of interest in relation to the current study, including financial, personal, authorship, or any other, that could affect the study, as well as the results reported in this paper.

Funding

The study was conducted without financial support.

Data availability

All data are available, either in numerical or graphical form, in the main text of the manuscript.

Use of artificial intelligence

The authors confirm that they did not use artificial intelligence technologies when creating the current work.

References

1. Wheeler, L., Dotson, J., Aftosmis, M., Coates, A., Chomette, G., Mathias, D. (2024). Risk assessment for asteroid impact threat scenarios. Acta Astronautica, 216, 468–487. https://doi.org/10.1016/j.actaastro.2023.12.049
2. Troianskyi, V., Kankiewicz, P., Oszkiewicz, D. (2023). Dynamical evolution of basaltic asteroids outside the Vesta family in the inner main belt. Astronomy & Astrophysics, 672, A97. https://doi.org/10.1051/0004-6361/202245678

3. Troianskyi, V., Godunova, V., Serebryanskiy, A., Aimanova, G., Franco, L., Marchini, A. et al. (2024). Optical observations of the potentially hazardous asteroid (4660) Nereus at opposition 2021. Icarus, 420, 116146. https://doi.org/10.1016/j.icarus.2024.116146
4. Khalil, M., Said, M., Osman, H., Ahmed, B., Ahmed, D., Younis, N. et al. (2019). Big data in astronomy: from evolution to revolution. International Journal of Advanced Astronomy, 7 (1), 11–14. https://doi.org/10.14419/ijaa.v7i1.18029
5. Adam, G. K., Kontaxis, P. A., Doulos, L. T., Madias, E.-N. D., Bouroussis, C. A., Topalis, F. V. (2019). Embedded Microcontroller with a CCD Camera as a Digital Lighting Control System. Electronics, 8 (1), 33. https://doi.org/10.3390/electronics8010033
6. Vavilova, I., Pakuliak, L., Babyk, I., Elyiv, A., Dobrycheva, D., Melnyk, O. (2020). Surveys, Catalogues, Databases, and Archives of Astronomical Data. Knowledge Discovery in Big Data from Astronomy and Earth Observation, 57–102. https://doi.org/10.1016/b978-0-12-819154-5.00015-1
7. Zhang, Y., Zhao, Y., Cui, C. (2002). Data mining and knowledge discovery in database of astronomy. Progress in Astronomy, 20 (4), 312–323.
8. Chalyi, S., Levykin, I., Biziuk, A., Vovk, A., Bogatov, I. (2020). Development of the technology for changing the sequence of access to shared resources of business processes for process management support. Eastern-European Journal of Enterprise Technologies, 2 (3 (104)), 22–29. https://doi.org/10.15587/1729-4061.2020.198527
9. Khlamov, S., Savanevych, V., Tabakova, I., Trunova, T. (2022). The astronomical object recognition and its near-zero motion detection in series of images by in situ modeling. 2022 29th International Conference on Systems, Signals and Image Processing (IWSSIP). https://doi.org/10.1109/iwssip55020.2022.9854475
10. Oszkiewicz, D., Troianskyi, V., Galád, A., Hanuš, J., Ďurech, J., Wilawer, E. et al. (2023). Spins and shapes of basaltic asteroids and the missing mantle problem. Icarus, 397, 115520. https://doi.org/10.1016/j.icarus.2023.115520
11. Savanevych, V., Khlamov, S., Briukhovetskyi, O., Trunova, T., Tabakova, I. (2023). Mathematical Methods for an Accurate Navigation of the Robotic Telescopes. Mathematics, 11 (10), 2246. https://doi.org/10.3390/math11102246
12. Bellanger, M. (2024). Digital Signal Processing. Wiley. https://doi.org/10.1002/9781394182695
13. Savanevych, V., Khlamov, S., Vlasenko, V., Deineko, Z., Briukhovetskyi, O., Tabakova, I., Trunova, T. (2022). Formation of a typical form of an object image in a series of digital frames. Eastern-European Journal of Enterprise Technologies, 6 (2 (120)), 51–59. https://doi.org/10.15587/1729-4061.2022.266988
14. Chen, S., Feng, H., Pan, D., Xu, Z., Li, Q., Chen, Y. (2021). Optical Aberrations Correction in Postprocessing Using Imaging Simulation. ACM Transactions on Graphics, 40 (5), 1–15. https://doi.org/10.1145/3474088
15. Klette, R. (2014). Concise computer vision. An Introduction into Theory and Algorithms. Springer. https://doi.org/10.1007/978-1-4471-6320-6
16. Khlamov, S., Tabakova, I., Trunova, T. (2022). Recognition of the astronomical images using the Sobel filter. 2022 29th International Conference on Systems, Signals and Image Processing (IWSSIP). https://doi.org/10.1109/iwssip55020.2022.9854425
17. Lösler, M., Eschelbach, C., Riepl, S. (2018). A modified approach for automated reference point determination of SLR and VLBI telescopes. Tm - Technisches Messen, 85 (10), 616–626. https://doi.org/10.1515/teme-2018-0053
18. Dhanalakshmi, R., Bhavani, N. P. G., Raju, S. S., Shaker Reddy, P. C., Mavaluru, D., Singh, D. P., Batu, A. (2022). Onboard Pointing Error Detection and Estimation of Observation Satellite Data Using Extended Kalman Filter. Computational Intelligence and Neuroscience, 2022, 1–8. https://doi.org/10.1155/2022/4340897
19. Krishnan, A. P., Belthangady, C., Nyby, C., Lange, M., Yang, B., Royer, L. A. (2020). Optical Aberration Correction via Phase Diversity and Deep Learning. https://doi.org/10.1101/2020.04.05.026567
20. Khlamov, S., Vlasenko, V., Savanevych, V., Briukhovetskyi, O., Trunova, T., Chelombitko, V., Tabakova, I. (2022). Development of computational method for matched filtration with analytical profile of the blurred digital image. Eastern-European Journal of Enterprise Technologies, 5 (4 (119)), 24–32. https://doi.org/10.15587/1729-4061.2022.265309
21. Khlamov, S., Savanevych, V., Vlasenko, V., Briukhovetskyi, O., Trunova, T., Levykin, I. et al. (2023). Development of the matched filtration of a blurred digital image using its typical form. Eastern-European Journal of Enterprise Technologies, 1 (9 (121)), 62–71. https://doi.org/10.15587/1729-4061.2023.273674
22. Burger, W., Burge, M. J. (2022). Digital Image Processing. In Texts in Computer Science. Springer International Publishing. https://doi.org/10.1007/978-3-031-05744-1
23. Vlasenko, V., Khlamov, S., Savanevych, V. (2024). Devising a procedure for the brightness alignment of astronomical frames background by a high frequency filtration to improve accuracy of the brightness estimation of objects. Eastern-European Journal of Enterprise Technologies, 2 (2 (128)), 31–38. https://doi.org/10.15587/1729-4061.2024.301327
24. Vlasenko, V., Khlamov, S., Savanevych, V., Trunova, T., Deineko, Z., Tabakova, I. (2024). Development of a procedure for fragmenting astronomical frames to accelerate high frequency filtering. Eastern-European Journal of Enterprise Technologies, 3 (9 (129)), 70–77. https://doi.org/10.15587/1729-4061.2024.306227
25. Rattanasoon, S., Semenko, E., Mkrtichian, D., Poshyachinda, S. (2024). Spectroscopic Devices for Asteroseismology With Small Telescopes in NARIT. Bulletin de La Société Royale Des Sciences de Liège, 96–101. https://doi.org/10.25518/0037-9565.11612
26. Kudzej, I., Savanevych, V. E., Briukhovetskyi, O. B., Khlamov, S. V., Pohorelov, A. V., Vlasenko, V. P. et al. (2019). CoLiTecVS – A new tool for the automated reduction of photometric observations. Astronomische Nachrichten, 340 (1-3), 68–70. https://doi.org/10.1002/asna.201913562

27. Troianskyi, V., Kashuba, V., Bazyey, O., Okhotko, H., Savanevych, V., Khlamov, S., Briukhovetskyi, A. (2023). First reported observation of asteroids 2017 AB8, 2017 QX33, and 2017 RV12. Contributions of the Astronomical Observatory Skalnaté Pleso, 53 (2). https://doi.org/10.31577/caosp.2023.53.2.5
28. Kudak, V. I., Epishev, V. P., Perig, V. M., Neybauer, I. F. (2017). Determining the orientation and spin period of TOPEX/Poseidon satellite by a photometric method. Astrophysical Bulletin, 72 (3), 340–348. https://doi.org/10.1134/s1990341317030233
29. Khlamov, S., Savanevych, V., Briukhovetskyi, O., Trunova, T. (2023). Big Data Analysis in Astronomy by the Lemur Software. 2023 IEEE International Conference on Information and Telecommunication Technologies and Radio Electronics (UkrMiCo). https://doi.org/10.1109/ukrmico61577.2023.10380398
30. Khlamov, S., Savanevych, V., Tabakova, I., Kartashov, V., Trunova, T., Kolendovska, M. (2024). Machine Vision for Astronomical Images using The Modern Image Processing Algorithms Implemented in the CoLiTec Software. Measurements and Instrumentation for Machine Vision, 269–310. https://doi.org/10.1201/9781003343783-12
31. Dougherty, E. R. (2020). Digital Image Processing Methods. CRC Press. https://doi.org/10.1201/9781003067054
32. Gonzalez, R., Woods, R. (2018). Digital image processing. Pearson. Available at: https://dl.icdst.org/pdfs/files4/01c56e081202b62bd7d3b4f8545775fb.pdf
33. Khlamov, S., Savanevych, V., Briukhovetskyi, O., Tabakova, I., Trunova, T. (2022). Astronomical Knowledge Discovery in Databases by the CoLiTec Software. 2022 12th International Conference on Advanced Computer Information Technologies (ACIT). https://doi.org/10.1109/acit54803.2022.9913188
34. Shvedun, V. O., Khlamov, S. V. (2016). Statistical modeling for determination of perspective number of advertising legislation violations. Actual Problems of Economics, 184 (10), 389–396.
35. Perova, I., Brazhnykova, Y., Miroshnychenko, N., Bodyanskiy, Y. (2020). Information Technology for Medical Data Stream Mining. 2020 IEEE 15th International Conference on Advanced Trends in Radioelectronics, Telecommunications and Computer Engineering (TCSET). https://doi.org/10.1109/tcset49122.2020.235399